Can the Western Boundary Layer Affect the Potential Vorticity Distribution in the Sverdrup Interior of a Wind Gyre?[1]

G. R. IERLEY[2]

Department of Mathematics, Massachusetts Institute of Technology, Cambridge, MA 02139

W. R. YOUNG[3]

Department of Physical Oceanography, Woods Hole Oceanographic Institution, Woods Hole, MA 02543

(Manuscript received 23 November 1982, in final form 31 May 1983)

ABSTRACT

The question posed in the title of this paper is answered in the affirmative by investigating a two-layer, quasi-geostrophic model of the wind-driven circulation. The two layers model the thermocline rather than the whole depth of the ocean. The wind stress is balanced by interfacial and bottom drag. This is perhaps the simplest baroclinic extension of Stommel's (1948) barotropic circulation model. It differs from an earlier model of Welander (1966) in that the vortex stretching nonlinearity is of primary importance.

In this model the dynamics of the frictional western boundary layer determine the vertical structure of the wind-driven flow in the Sverdrup interior. Thus, in a sense, the boundary layer is "active" and cannot be appended to an arbitrary interior flow; rather it partially determines the interior circulation by setting the functional relationship between the streamfunction and the potential vorticity in the lower layer.

In previous studies (Rhines and Young, 1982b) this functional relationship has been calculated using a generalized Prandtl–Batchelor theorem. This result does not apply to the present calculation because every lower layer streamline passes through a frictional boundary layer.

1. Introduction

It seems overwhelmingly likely that the answer to the question posed in the title of this paper is "yes" and this is, in fact, our conclusion. A little reflection, however, shows, that there are no previous theories which directly address this issue. For instance, in all homogeneous circulation theories, the potential vorticity in the Sverdrup interior is prescribed at the outset, i.e.,

$$q = f/H,$$

where $H(x, y)$ is the depth of the ocean. In these theories the potential vorticity distribution is unaltered by the flow in general and the western boundary layer in particular.

In baroclinic circulation theories, the potential vorticity distribution departs markedly from the environmental distribution because of vortex stretching. For instance, in Needler's (1967) thermocline theory, the potential vorticity is uniform on density surfaces. In this particular theory, as in most similarity solutions, the distribution is specified *a priori* by the theorist, and analytic tractability, rather than physical considerations, governs the choice.

By contrast, Rhines and Young (1982a) construct a circulation theory in which a particular physical process (down-gradient flux of mean potential vorticity due to mesoscale eddies) determines the potential vorticity distribution. The western boundary layer per se is not implicated in this process although one has to make some rather strong assumptions (see discussion below) about its dynamics in order to apply the quasi-geostrophic version of the Prandtl-Batchelor theorem given by Rhines and Young (1982b).

In this article we use a simple two-layer extension of Stommel's (1948) homogeneous model. The two layers are intended to represent the density structure of the upper thermocline rather than the full depth of the ocean. They are bounded below by a thick, deep layer which is motionless in the Sverdrup interior.

Our model uses the two-layer quasi-geostrophic approximation (Pedlosky, 1979). It is wind-driven and dissipation is provided by vertical friction. Relative vorticity is ignored, even in the western boundary layer. The only nonlinearity then is the vortex stretching produced by deformation of the interface between the layers.

[1] Contribution of the Scripps Institution of Oceanography, new series.

[2] Present affiliation: Dept. of Mathematics and Computer Sciences, Michigan Technological University, Houghton, MI 49931.

[3] Present affiliation: University of California, San Diego, Marine Physical Laboratory of the Scripps Institution of Oceanography, La Jolla, CA 92093.

This model is similar to that of Welander (1966). It differs in that we use the quasi-geostrophic approximation and discuss the consequences of the vortex stretching nonlinearity both in the Sverdrup interior and in the western boundary layer. Welander (1966) avoided the quasi-geostrophic approximation and allowed the density interface to undergo large vertical excursions and even surface. He assumed that the lower layer is much thicker than the upper layer, since this allows the rigorous neglect of the vortex stretching nonlinearity. This restriction also ensures that the fractional depth changes in the lower layer are small so that the lower layer geostrophic contours are dominated by the β-effect. Thus all the geostrophic contours intersect the eastern boundary so that the general results of Rhines and Holland (1979) and Rooth *et al.* (1978) show that there is no lower layer flow in the Sverdrup interior. In the western boundary layer, however, the stresses are large enough to drive a frictional boundary layer in the lower layer. Welander's solution is summarized in Fig. 1. In Welander's model the two layers represent the full depth of the ocean. A very thick lower layer is then a natural assumption. In the present model the two layers represent the thermocline waters, and so correspond to the upper layer of Welander's model. Thus, in a sense, we are investigating the consequences of increasing the vertical resolution of the thermocline in Welander's model.

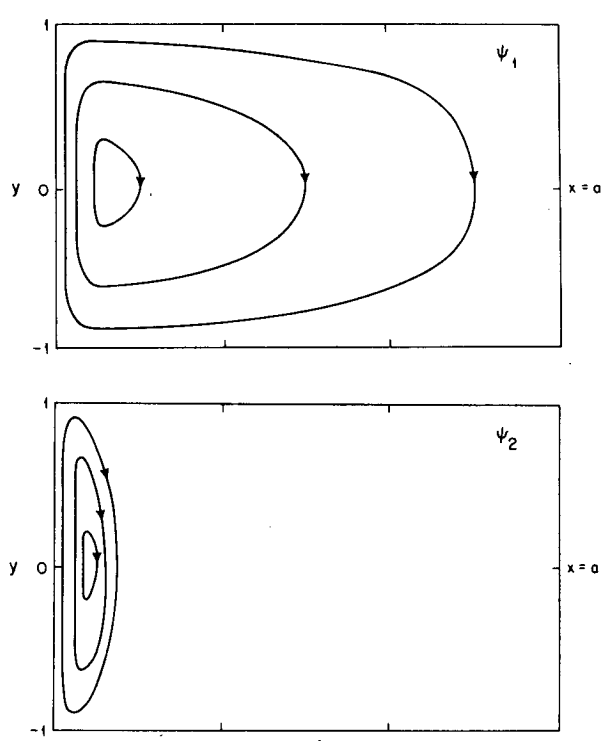

FIG. 1. A schematic illustration of the streamfunctions ψ_1 and ψ_2 when the vortex stretching nonlinearity is absent ($F = 0$). As in Welander (1966) ψ_2 is essentially zero in the Sverdrup interior and all of the transport is in the upper layer.

Increased vertical resolution in this region produces qualitatively new phenomena: stretching distorts the lower thermocline layer geostrophic contours to the extent that they close and no longer intersect the eastern boundary. As in Rhines and Young (1982a; hereafter RY) and Young and Rhines (1982; hereafter YR), this allows substantial flows to develop in parts of the lower thermocline layer Sverdrup interior. The present model differs from RY and YR in that the potential vorticity homogenization results of Rhines and Young (1982b) are inapplicable. This is because every streamline passes through a frictional boundary layer where the streamfunction ψ_2 and the potential vorticity q_2 are not functionally related. Because the quasi-geostrophic version of the Prandtl–Batchelor theorem given by Rhines and Young (1982b) requires

$$q_2 = Q(\psi_2) \tag{1.1}$$

everywhere on a closed streamline, the potential vorticity is not uniform inside closed geostrophic contours. The major theme of this paper is that (1.1) remains valid in the Sverdrup interior and Q is determined by the dynamics of the frictional boundary layer where (1.1) itself is invalid. Thus in the model discussed here the frictional western boundary layer cannot be appended to an arbitrary interior flow; rather, it determines the vertical structure of the interior Sverdrup flow by setting the functional relationship between ψ_2 and q_2 in the Sverdrup interior.

2. Formulation—the two-layer quasi-geostrophic model

Throughout the article we use the two-layer quasi-geostrophic approximation (Pedlosky, 1979). Relative vorticity is ignored even in the boundary layer, as in the simple but self-consistent models of Munk (1950) and Stommel (1948). The parameter range in which the neglect is rigorously justified is probably not directly relevant to either the ocean or eddy resolving general circulation models such as Holland (1983). Direct applicability to other systems is not, however, the primary purpose of models such as these. The limited goal of understanding them on their own terms is a useful intuition building exercise because it focuses our attention on a specific process [in this case vertical stress transmission in a western boundary layer and how it affects the Sverdrup interior by determining Q in (1.1)].

a. The dimensional equations of motion

The dimensional two-layer quasi-geostrophic equations are

$$J(\psi_1, q_1) = (f_0 w_E/H) + \nu\nabla^2(\psi_2 - \psi_1), \tag{2.1a}$$

$$J(\psi_2, q_2) = \nu\nabla^2(\psi_1 - \psi_2) - \delta\nabla^2\psi_2, \qquad (2.1b)$$

where ψ_n is a streamfunction, q_n the potential vorticity, w_E the Ekman pumping and

$$J(A, B) = \frac{\partial A}{\partial x}\frac{\partial B}{\partial y} - \frac{\partial A}{\partial y}\frac{\partial B}{\partial x}$$

is a horizontal Jacobian. The potential vorticities are given by

$$q_1 = \beta y + F(\psi_2 - \psi_1), \qquad (2.2a)$$

$$q_2 = \beta y + F(\psi_1 - \psi_2), \qquad (2.2b)$$

where β is the north–south gradient of the Coriolis frequency, i.e.,

$$f = f_0 + \beta y, \qquad (2.3a)$$

$$F = f_0^2/g'H, \qquad (2.3b)$$

where g' is the reduced gravity between the two upper layers and H is the depth of each layer. For simplicity we have made the nonessential assumption that the layers have equal depths.

In (2.1) ν is an interfacial drag which transfers momentum vertically between the layers, and δ is drag on the bottom or on a motionless deep third layer.

In Welander's two-layer model, the two layers comprised the full vertical extent of the ocean. Here the two layers are intended to model the upper thermocline waters which contain the wind gyre (see RY and YR for scale estimates of the depth of the wind gyre using a continuously stratified model). Thus the two layers here correspond to the upper layer of Welander's model. A three-layer model reduces to a two-layer model such as (2.1), if one allows the fraction of the depth occupied by the deepest layer to approach unity and also increases the density jump between the middle and deepest layer. In this limit it is physically intuitive that the lowest layer is at rest and acts as an "effective" bottom for the two layers above. In fact, it is easy to show that the precise condition on the external parameters which justifies this reduction from three to two layers is

$$g'' \gg g',$$

where g'' is the reduced gravity between the middle and bottom layer.

b. Non-dimensionalization

We will temporarily denote non-dimensional quantities by an asterisk. The scaling adopted is

$$(x, y) = L(x_*, y_*), \qquad (2.4a)$$

$$\psi_n = UL\psi_{*n}, \qquad (2.4b)$$

$$q = \beta L q_*, \qquad (2.4c)$$

$$w_E = W w_{E*}, \qquad (2.4d)$$

$$(\nu, \delta) = \beta L(\nu_*, \delta_*), \qquad (2.4e)$$

where $2L$ is the north–south width of the basin and U is a typical horizontal velocity. The Sverdrup balance determines U in terms of external variables:

$$U = f_0 W/\beta H. \qquad (2.5)$$

The non-dimensional version of (2.1) and (2.2) is

$$J(\psi_{1*}, q_{1*}) = w_{E*} + \nu_*\nabla_*^2(\psi_{2*} - \psi_{1*}), \qquad (2.6a)$$

$$J(\psi_{2*}, q_{2*}) = \nu_*\nabla_*^2(\psi_{1*} - \psi_{2*}) - \delta_*\nabla_*^2\psi_{2*}, \qquad (2.6b)$$

$$q_{1*} = y_* + F_*(\psi_{2*} - \psi_{1*}), \qquad (2.6c)$$

$$q_{2*} = y_* + F_*(\psi_{1*} - \psi_{2*}), \qquad (2.6d)$$

$$F_* = FU/\beta. \qquad (2.6e)$$

We will suppose that the friction is weak so ν_* and δ_* are very small.

3. Theoretical analysis

a. The barotropic mode equation

We begin by forming the equation for the barotropic mode. We add (2.6a) to (2.6b) to obtain

$$\frac{\partial\psi_B}{\partial x} = w_E - \delta\nabla^2\psi_2, \qquad (3.1a)$$

$$\psi_B = \psi_1 + \psi_2, \qquad (3.1b)$$

where we have now dropped the asterisks. Note how the large nonlinear vortex stretching terms cancel. In the Sverdrup interior, outside the frictional western boundary layers, the last term in (3.1a) is small and

$$\psi_B = (x - a)w_E(y), \qquad (3.2)$$

where $x = a$ is the eastern boundary. In Fig. 2 we show ψ_B when

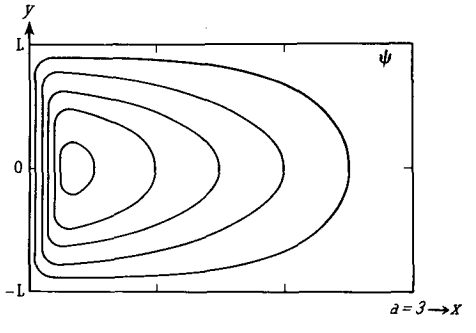

FIG. 2. The barotropic streamfunction ψ_B. The western boundary layer is schematic while the interior pattern is calculated from (3.2).

$$w_E = -\cos(\tfrac{1}{2}\pi y) \tag{3.3}$$

and $a = 3$. The choice (3.3) models Ekman pumping in a subtropical wind gyre.

b. An equation for ψ_2 and ψ_B

Using (3.1b) one can eliminate ψ_1 from (2.6b) to obtain

$$J(\psi_2, q) = \nu\nabla^2\psi_B - (2\nu + \delta)\nabla^2\psi_2, \tag{3.4a}$$

$$q \equiv y + F\psi_B. \tag{3.4b}$$

Eq. (3.4a) is an advection-diffusion equation in which $\nu\nabla^2\psi_B$ is a source term. It is intuitively useful to think of q as a streamfunction producing a velocity $\mathbf{z} \times \nabla q$ which advects the "passive scalar" ψ_2. The "streamlines" are sketched in Fig. 3 for various values of F. This interpretation in terms of an advection-diffusion equation is a generalized version of Welander's (1968) thermal analogy.

The details of the western boundary layer are not shown in this figure. It is clear, however, that since $\psi_B = 0$ on the boundary, a q contour which starts at y_* on the eastern boundary must also hit the western boundary at y_*. This ensures that the horseshoe-shaped contours in Fig. 3 close in the boundary layer as shown schematically in Fig. 4.

c. The limit $F \ll 1$

For orientation it is useful to first consider $F \ll 1$ so that

$$q = y \tag{3.5}$$

and (3.1a) and (3.4a) are linear. The solution of these equations is shown schematically in Fig. 1. The limit $F \ll 1$ corresponds to the case studied by Welander (1966, 1968). In the Sverdrup interior ψ_2 is very small (order ν) because the eastern boundary condition

$$\psi_2 = 0, \tag{3.6}$$

together with the interior solution of (3.4a)

$$\psi_2 = G(q) + O(\nu), \tag{3.7}$$

implies

$$G = 0. \tag{3.8}$$

This argument relies on the fact that q is dominated by y so all q contours intersect the eastern boundary where (3.6) applies. However, when F is O(1) there is a pocket of closed q contours in the northwest corner of the basin (see Fig. 3). In this region (3.8) is not forced by the boundary conditions and O(1) lower layer flows can exist.

d. The extent of the region of closed q contours

We saw above that when a point in the interior is threaded by a q contour which leads back to the eastern boundary there can be only weak flows at that point. Thus our attention is now focused on the closed contours in the northwest corner of the basin where the boundary conditions (3.6) do not preclude the existence of order one velocities.

The size of this region may be gauged by noting that if the Ekman velocity is given by (3.3) then the outermost closed q contour (*i.e.*, $q = 1$) intersects the northern boundary at

$$x_N = a - (2/\pi F).$$

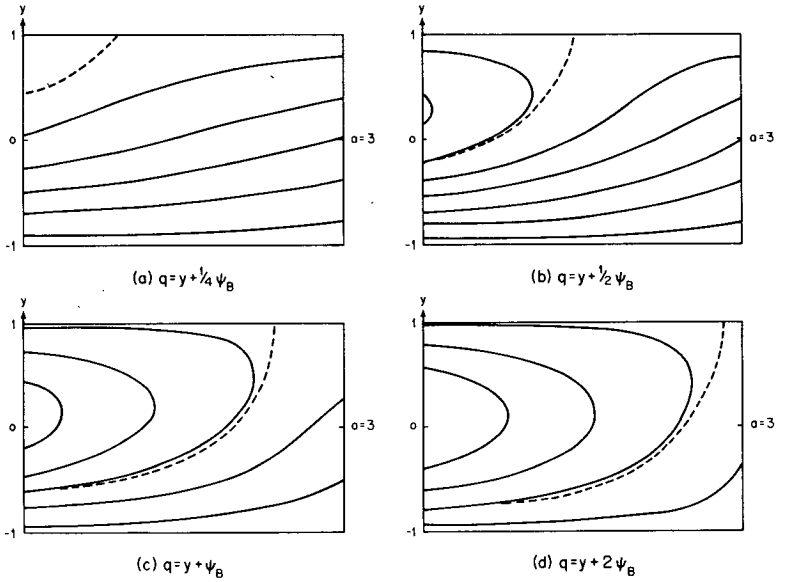

FIG. 3. The lower layer geostrophic contours $q = y + F\psi_B$, for various values of F. The outermost closed contour (dashed) is $q = 1$. The contours which strike the eastern boundary $x = a = 3$, are referred to as blocked.

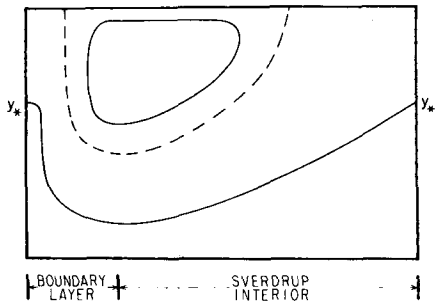

FIG. 4. A schematic illustration of the way the contours in Fig. 3 must close in the western boundary layer. Because ψ_B is zero on the boundary, a blocked contour which starts at y_* on the eastern boundary must also intersect the western boundary at y_*.

If closed contours are to exist, then this point must lie in the basin and so F must be greater than $(2/\pi a)$. Now suppose that $H = 400$ m, $g' = 0.5$ cm s^{-2}, $f_0 = 10^{-4}$ s^{-1}, $\beta = 1.6 \times 10^{-13}$ cm^{-1} s^{-1}, $U = 1$ cm s^{-1}, then from (2.3b) and (2.6e)

$$x_N = a - \frac{1}{5},$$

so that if $a = 3$, as in Figs. 1–3, then the contour $q = 1$ intersects the northern boundary very close to the eastern boundary and a large fraction of the lower layer must be within closed q contours. Of course if one increases the layer thickness or g', then this region becomes smaller but its extent changes continuously. This physically reasonable behavior should be contrasted with that in a model where $F \equiv 0$. In that case the total Sverdrup transport is always in the top layer no matter how small H and g'.

e. *Inapplicability of the generalized Prandtl–Batchelor theorem*

When $F\psi_B$ in (3.4b) is large enough to overpower y, the q contours (which are essentially geostrophic contours) close in the northwest corner of the gyre. It is in these closed regions that RY and YR applied the generalized Prandtl–Batchelor theorem to calculate G in (3.7). In the present problem this theorem leads to (see Appendix A)

$$\psi_2 = \left(\frac{\nu}{2\nu + \delta}\right)[(y/F) + \psi_B] \text{ (wrong)}. \qquad (3.9)$$

The above result is incorrect because the theorem is inapplicable. The derivation in Appendix A assumes that (3.7) applies *everywhere* around a closed q contour. In the Sverdrup interior, (3.7) is correct because the dissipative terms on the rhs of (3.4a) are small. In the frictional western boundary layer, however, these terms are large.

Nevertheless, one might hope that (3.9) is fortuitously correct, since it is an exact solution of (3.4a) inside the closed q contours, where it doesn't violate the boundary condition

$$\psi_2 = 0.$$

This specious argument was advanced by Young (1980). The numerical solutions presented in Section 4 show conclusively that (3.9) is wrong and unequivocally support the simple theory presented in the next subsection.

f. *Solution of (3.4a) in the Sverdrup interior*

In the interior, the terms on the rhs of (3.4a) are small and

$$\psi_2 = G(q) + O(\nu, \delta). \qquad (3.10)$$

In blocked regions, where q contours lead back to the eastern boundary, $G = 0$. In the closed region we will show that G is determined by conditions at the outer edge of the northern boundary layer where fluid enters the interior.

g. *Solution of (3.4a) in the northern boundary layer where flow is into the interior*

First, we consider the northern section of the boundary layer where fluid is leaving the boundary layer and entering the interior. For a general w_E this northern exit region is the region in which $\partial[y - aFw_E(y)]/\partial y < 0$.

The form of (3.4a) suggests the "ansatz"

$$\psi_2 = \lambda\psi_B, \qquad (3.11)$$

where λ is a constant to be determined. Substituting (3.11) into (3.1a) and neglecting terms of $O(\delta, \nu)$ gives

$$\frac{\partial\psi_B}{\partial\xi} = -\lambda\frac{\partial^2\psi_B}{\partial\xi^2}, \qquad (3.12)$$

where

$$\xi \equiv x/\delta$$

is a boundary layer coordinate.

Substituting (3.11) into (3.4a) gives

$$\lambda\frac{\partial\psi_B}{\partial\xi} = [\alpha - \lambda(2\alpha + 1)]\frac{\partial^2\psi_B}{\partial\xi^2}, \qquad (3.13)$$

where

$$\alpha \equiv \nu/\delta = O(1). \qquad (3.14)$$

If the ansatz (3.11) is to work, then (3.12) and (3.13) must be the same equation. This condition leads to

$$\lambda^2 - (1 + 2\alpha)\lambda + \alpha = 0. \qquad (3.15)$$

This quadratic has two solutions but only

$$\lambda = [1 + 2\alpha - (1 + 4\alpha^2)^{1/2}]/2 \qquad (3.16)$$

gives a physically acceptable solution.

The behavior of λ as α is varied is interesting. If $\alpha \to \infty$, so that interfacial friction overpowers drag,

$\lambda \to 1/2$. From (3.11) this means that the boundary layer flow is barotropic as intuition suggests. If $\alpha \to 0$, so the interfacial friction is weak, $\lambda \to \alpha \ll 1$. This means that the lower layer flow is weak, again as one might have anticipated intuitively.

h. Calculation of G by matching

We now calculate G in (3.10) by requiring that the boundary layer solutions obtained from (3.11) and (3.12),

$$\psi_2 = -\lambda a(1 - e^{-x/\lambda\delta})w_E(y) \tag{3.17}$$

and the interior solution

$$\psi_2 = G[y + F(x - a)w_E(y)], \tag{3.18}$$

match in the intermediate region

$$\frac{x}{\delta} \gg 1, \quad x \ll 1. \tag{3.19}$$

Thus G is calculated by the elimination of y between (3.17) and (3.18) using (3.19).

Suppose for example that

$$w_E = -\cos(\pi y/2), \tag{3.20}$$

then

$$G^{-1}(\psi_2) = (2/\pi)\cos^{-1}(\psi_2/\lambda a) + (F/\lambda)\psi_2. \tag{3.21}$$

With the forcing function (3.20) it is impossible to give an explicit expression for G itself. This is not important, however, since by comparing the theory with the numerical solutions, one can plot the function

$$q - G^{-1}(\psi_2),$$

where G^{-1} is defined in (3.21). We expect that

$$q - G^{-1}(\psi_2) = (q - 1)$$

in the blocked regions where $\psi_2 = 0$, (3.22a)

and

$$q - G^{-1}(\psi_2) = 0 \text{ in the closed regions.} \tag{3.22b}$$

Finally, although it is not possible to invert (3.21) exactly, it is easy to obtain a very accurate approximation by reversion of the Taylor series

$$\cos^{-1}(s) = \frac{\pi}{2} - s - \frac{1}{6}s^3 + \cdots.$$

One finds

$$\left(\frac{aF - 1}{\lambda a}\right)\psi_2 = (q - 1) + \frac{1}{3\pi}\left(\frac{q - 1}{aF - 1}\right)^3 + \cdots.$$

Because the largest value of q in the basin is aF the cubic term is always less than $(3\pi)^{-1}$ and can usually be neglected. Thus there is approximately a linear relation between ψ_2 and q within the closed contours.

i. Discussion of (3.4a) in the southern boundary layer where flow is out of the interior

We have been unable to provide a simple analytic description of the southern boundary layer region where $\partial[y - aFw_E(y)]/\partial y > 0$. This is the region where fluid is flowing out of the Sverdrup interior and into the western boundary layer. In theories which include relative vorticity this is the region where an inertial boundary layer forms (*e.g.*, Pedlosky, 1979, Section 5.6; and YR). It is ironic that in the simple frictional model used here, this region apparently has more complicated dynamics. Since the numerical calculations described in the next section confirm the theoretical analysis previously presented, we have not attempted to provide a detailed theoretical discussion of this region. One should probably regard the argument leading to (3.21) as a plausible heuristic assertion which must be computationally verified.

There is, however, a simple analytic argument which is informative. If we consider the approximate form of (3.4a) in the intermediate region $\xi = x/\delta \gg 1$ and $x \ll 1$ to be explicit, we could take $x = O(\delta^{1/2})$. In this intermediate region, the boundary correction to the interior solution is small. It is then straightforward to obtain a linear, ordinary differential equation in x for the boundary-layer correction, by linearizing (3.4a) about the interior solution. The coefficients of this ordinary differential equation depend on y parametrically.

One finds that in the southern region, where fluid enters the boundary layer and $q_y > 0$, all of the solutions of this ordinary differential equation remain bounded as $x \to \infty$. Thus in this southern region it is possible in principle to construct a solution which matches an arbitrary interior ψ_2 and also satisfies the boundary condition at $x = 0$. Thus the southern boundary layer is "passive"; it can be appended to an arbitrary interior flow.

In the northern region, where fluid is flowing out of the boundary layer and $q_y < 0$, one of the solutions of the ordinary differential equation grows exponentially as $x \to \infty$. Thus this particular function must be excluded from the solution. This means that only the boundary condition at $x = 0$ can be satisfied. In fact, as we have seen, the interior ψ_2 is determined by the limiting behavior of the boundary layer solution as $x \to \infty$. In this sense the northern boundary layer is "active"; it determines the interior flow.

j. The limit $F \gg 1$, $(\delta/\nu) \ll 1$

Finally, it is interesting to note that in the limit above the two layers are locked together and behave as one. Note that *both* conditions are required: $F \gg 1$ ensures that closed q contours occupy almost the whole basin and $(\delta/\nu) \ll 1$ ensures that

$$\psi_1 = \psi_2 + O(\delta/\nu).$$

This limit is potentially interesting because it suggests that the layers of finite thickness may be more than just a convenient mathematical approximation. Weak interfacial friction and strong nonlinearity can conspire to couple several thin layers so that they behave as a single thicker layer. Indeed, one may speculate that because of this process, a continuous density profile effectively behaves like a finite number of layers.

4. Description of the numerical methods

For the purposes of numerical solution we consider the time-dependent version of (2.6a, b)

$$q_{1t} + J(\psi_1, q_1) = w_E + \nu\nabla^2(\psi_2 - \psi_1), \tag{4.1a}$$

$$q_{2t} + J(\psi_2, q_2) = \nu\nabla^2(\psi_1 - \psi_2) - \delta\nabla^2\psi_2, \tag{4.1b}$$

and form the equation for the baroclinic mode

$$\vartheta = \psi_1 - \psi_2 \tag{4.2}$$

by subtracting (4.1b) from (4.1a) with the result

$$2F\frac{\partial\vartheta}{\partial t} + J(q, \vartheta) = -w_E - \frac{\delta}{2}\nabla^2\psi_B + \left(2\nu + \frac{\delta}{2}\right)\nabla^2\vartheta. \tag{4.3}$$

The neglect of relative vorticity leaves Eq. (3.1a) for the barotropic mode unchanged, *i.e.*, barotropic adjustments occur instantaneously in this approximation.

Solutions of (3.1a) and (4.3) are represented in the form

$$\begin{Bmatrix}\psi_B\\ \vartheta\end{Bmatrix} = \sum_{i=0}^{32}\sum_{j=0}^{16}\begin{Bmatrix}\psi_B\\ \vartheta\end{Bmatrix}_{ij}(t)T_i(z(x))T_j(y). \tag{4.4}$$

The western boundary layer imposes stringent requirements on resolution in x. If we take $\vartheta = 0$ initially, then a substitution in (3.1a) of the form

$$\psi_B = \psi_B(x)\cos(\pi y/2) \tag{4.5}$$

leads to the ordinary differential equation

$$\left(\frac{\delta}{2}\frac{d^2}{dx^2} + \frac{d}{dx} - \delta\frac{\pi^2}{8}\right)\psi_B = -1, \tag{4.6}$$

subject to homogeneous boundary conditions at $x = \pm 1$. (In describing the numerical solution it is convenient to rescale the x axis so it runs from -1 to 1.) For small δ, one of the homogeneous solutions is

$$\psi_B = \exp(-2x/\delta). \tag{4.7}$$

Expansion coefficients for the Chebyshev representation of (4.7) are given by

$$\psi_{Bn} = \frac{2}{\pi c_n}\int_{-1}^{1} T_n(x)e^{-2x/\delta}\frac{dx}{(1-x^2)^{1/2}}, \qquad c_n = \begin{cases}2, & n = 0\\ 1, & n > 0.\end{cases} \tag{4.8a}$$

The integral above is standard and one finds

$$\psi_{B_n} = \frac{2}{\pi c_n} I_n(2/\delta), \tag{4.8b}$$

where I_n is a modified Bessel function. [For steady-state solutions when ϑ is nonzero, using the relation $\psi_2 = \lambda\psi_B$ found in Section 3 changes this result to $I_n(1/\lambda\delta)$.] The behavior of the Bessel function for large arguments (small viscosity) leads to a flat spectrum which does not fall off until rather large values of the Chebyshev index n. We therefore adopted a simple mapping in x to stretch the boundary layer region, i.e.

$$z(x) = 2\left[\frac{1 - e^{-(x+1)/\nu'}}{1 - e^{-2/\nu'}}\right] - 1. \tag{4.9}$$

In (4.9), ν' is a free parameter which is adjusted to ensure stability and convergence of the numerical procedure. Hence,

$$\frac{\partial}{\partial x} \to \frac{1}{\nu'}(z^* - z)\frac{\partial}{\partial z}, \tag{4.10a}$$

where

$$z^* = \left[\frac{2}{1 - e^{-2/\nu'}} - 1\right]. \tag{4.10b}$$

Some experimentation to find the optimal mapping parameter resulted in the choice of $\nu' = 4\delta$. (Smaller values of ν' resulted in insufficient resolution of the interior.)

For time stepping, a Crank Nicholson leapfrog scheme was used, but for improved stability, a predictor-partial corrector refinement originally proposed by Gadzag (1976) was added. Specifically, the predictor step was

$$\frac{F}{\Delta t}\tilde{\vartheta}^{m+1} - \frac{1}{2}\left[\left(2\nu + \frac{\delta}{2}\right)\nabla^2\tilde{\vartheta}^{m+1} + \tilde{\vartheta}_x^{m+1}\right] = \frac{F}{\Delta t}\vartheta^{m-1} + \frac{1}{2}\left[\left(2\nu + \frac{\delta}{2}\right)\nabla^2\vartheta^{m-1} + \vartheta_x^{m-1}\right] - w_E + FJ(\tilde{\vartheta}^m, \psi_B{}^m), \tag{4.11a}$$

and a corrector step

$$\frac{2F}{\Delta t}\vartheta^{m+1} - \frac{1}{2}\left[\left(2\nu + \frac{\delta}{2}\right)\nabla^2\vartheta^{m+1} + \vartheta_x^{m+1}\right] = \frac{2F}{\Delta t}\vartheta^m + \frac{1}{2}\left[\left(2\nu + \frac{\delta}{2}\right)\nabla^2\vartheta^m + \vartheta_x^m\right] - w_E + \frac{F}{2}\left[J(\tilde{\vartheta}^{m+1}, \psi_B^{m+1}) + J(\tilde{\vartheta}^m, \psi_B^m)\right]. \tag{4.11b}$$

Most of the computation time is spent calculating $J(\tilde{\vartheta}^{m+1}, \psi_B^{m+1})$ in the corrector step, even with the use of a fast Fourier transform.

To facilitate solution of the implicit operator, a diagonalization scheme introduced by Haidvogel and Zang (1979) for the Poisson equation was used. Sym-

bolically, Eqs. (4.11a, b) (and the ψ_B equation) are in the form

$$\sum_j \mathbf{M}_{ij}\vartheta_{jk} + \sum_l \vartheta_{il}\mathbf{N}_{lk} = f_{ik}, \tag{4.12}$$

where $\mathbf{M}_{ij}$ is the matrix representing the operator

$$\left(2\nu + \frac{\delta}{2}\right)\frac{\partial^2}{\partial x^2} + \frac{\partial}{\partial x}, \tag{4.13}$$

or, in terms of the variable z,

$$\frac{(2\nu + \delta/2)}{\nu'^2}(z^* - z)^2\frac{\partial^2}{\partial z^2} + \frac{1}{\nu'}\left[1 - \frac{(2\nu + \delta/2)}{\nu'}\right](z^* - z)\frac{\partial}{\partial z}. \tag{4.14}$$

Explicit forms for these operators in Chebyshev space may be deduced from various recurrence relations and a useful compendium may be found in Gottlieb and Orszag (1977). The matrix $\mathbf{M}$ in the Haidvogel and Zang proposal is decomposed as

$$\mathbf{M} = \mathbf{e}\Lambda\mathbf{e}^{-1}, \tag{4.15}$$

where $\mathbf{e}$ is the eigenvector matrix, $\mathbf{e}^{-1}$ its inverse and Λ, the diagonal eigenvalue matrix. To apply their scheme, the (33×33) matrix form of $\mathbf{M}$ must first be reduced to (31×31) using the two highest Chebyshev coefficients to satisfy the homogeneous boundary conditions on ϑ, otherwise the eigenvalue spectrum is undetermined. Multiplying (4.12) from the left with $\mathbf{e}^{-1}$ we obtain

$$\Lambda_{il}\hat{\vartheta}_{ik} + \sum_l \hat{\vartheta}_{il}\mathbf{N}_{ik} = \hat{f}_{ik} \tag{4.16}$$

where

$$\hat{\vartheta}_{ik} = \sum_j \mathbf{e}^{-1}_{ij}\vartheta_{jk}$$

and similarly for $\hat{f}_{ik}$. The transformation of basis has diagonalized the equations in x. The remaining problem of 17 coupled linear equations in y can be solved rather easily because of the simple form of $\mathbf{N}$. An accurate and efficient procedure is briefly sketched in Gottlieb and Orszag (1977) for reducing the equations to a quasi-tridiagonal form which requires only about $5N$ operations to solve.

Several tests were made to ensure accuracy of the results. The numerical solution for the uncoupled barotropic equation was checked against the analytic result in the form (4.3). Also the lowest decay mode of the unforced, linear, baroclinic equation

$$\vartheta = e^{-5/3x}\cos\left(\frac{\pi}{2}x\right)\cos\left(\frac{\pi}{2}y\right)e^{-\mu t}, \tag{4.17a}$$

$$\mu = \frac{1}{16\nu_\vartheta F} + \frac{\nu_\vartheta\pi^2}{2F}, \quad \nu_\vartheta \equiv \left(2\nu + \frac{\delta}{2}\right), \tag{4.17b}$$

was used as an initial condition in time stepping. For $\nu_\vartheta = 0.15$, $F = 10$; $\mu = 0.11568871$ and with $\Delta t = 0.01$ this value obtained to the number of places shown as inferred from successive ratios of $\vartheta_{1,1}$ and $\vartheta_{10,5}$. Several equilibrated runs were stepped further using a true spectral calculation of the quadratic nonlinearity and aliasing errors were found to be negligible. Multiplying (4.3) by ϑ and (3.1a) by ψ_B and integrating over the domain, we obtain, after some simplification,

$$F\frac{\partial\langle\vartheta^2\rangle}{\partial t} = \frac{\delta}{2}\langle(\nabla\psi_B)^2\rangle + (2\nu + \delta/2) \times \langle(\nabla\vartheta)^2\rangle + \langle w_E(\psi_B - \vartheta)\rangle. \tag{4.18}$$

The quantity $(\langle\vartheta^2\rangle^{m+1} - \langle\vartheta^2\rangle^m)/\Delta t$ was found to agree with the right hand side to better than 0.5% for a single step. Finally, the ratios $\vartheta_{31,j}/\vartheta_{1,j}$ and $\vartheta_{i,15}/\vartheta_{i,1}$ were computed for the equilibrium solutions. The first of these was typically 1/500, the second about 10^{-4}.

5. Comparison of numerical results with theory

Five runs with various values of F and ν were made, all with $\delta = 0.1$, which represented the best approximation to the inviscid limit which could be achieved. In practice, eigenvector-eigenvalue computation failed somewhat before the Chebyshev resolution limit was reached so that there is a slight computational advantage in diagonalizing in y, but at the cost of added programming effort to solve the resulting linear system in x explicitly. The results presented here are for $F = 2$, $\delta = 0.1$ and $\nu = 0.05$. None of the other runs in this range showed larger variation from theory than the one presented here.

Figs. 5 and 6 show $[q - G^{-1}(\psi_2) + 1]$ where, in the first of these, the Prandtl–Batchelor theorem (3.9) was used to determine G^{-1}, while in the second, Eq. (3.21) was employed. The striking contrast of these figures makes it quite evident that the arguments advanced in Section 3 are correct and that the functional relation between ψ_2 and q is appreciably altered in the passage of streamlines through the western boundary layer. Fig. 7, which shows ψ_1, exhibits the north–south asymmetry produced by the compression of the lower layer circulation into the northwest corner of the basin. From Fig. 8, which illustrates ψ_2, one can see that the region over which $[q - G^{-1}(\psi_2)]$ is constant does coincide with the closed region outside of which ψ_2 is sensibly zero. Figs. 9 and 10 demonstrate the relation between ψ_2 and ψ_B at various latitudes. (That is, y is fixed and ψ_2 vs. ψ_B is plotted on a zonal section.) For $y > 0.4$ one can see that the linear relation in the boundary layer does not vary much as a function of latitude. In the northwest corner, the slope of 0.288 agrees quite well with the theoretical value of:

$$\lambda = 1 - \frac{1}{\sqrt{2}} \approx 0.293.$$

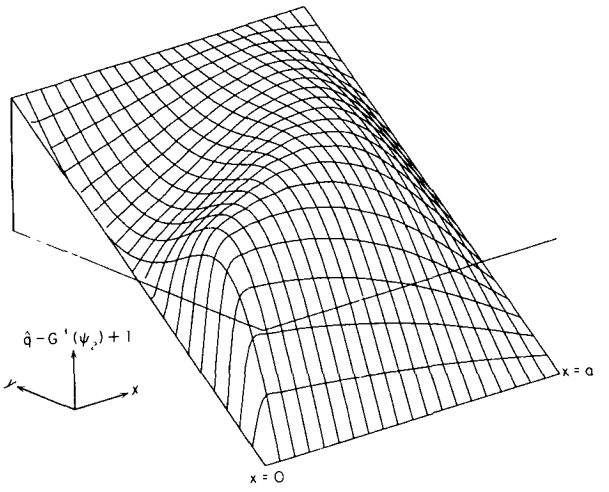

FIG. 5. $q - G^{-1}(\psi_2) + 1$ with G calculated by the incorrect application of the Prandtl-Batchelor theorem [see (3.9)]. If ψ_2 were correctly given in terms of q by (3.9), then the function in this figure would be flat in the northwest corner where the q contours close (cf., Fig. 6).

In the inviscid limit the relation of ψ_2 and ψ_B would appear as a triangular figure (see Fig. 11) whose base at $\psi_2 = 0$ extends from the eastern edge (where $\psi_B = 0$) to the border of the blocked region where $q = 1$. The boundary layer relation $\psi_2 = \lambda\psi_B$ extends from the origin to the point $[-aw_E(y), -\lambda aw_E(y)]$ and finally the closed interior joins this last point to $[(1 - y)/F, 0]$. The actual result for $y = 0.8$ shows this qualitative behavior, the gap between the smooth result and the limiting triangle disappearing as $(\nu, \delta) \to 0$.

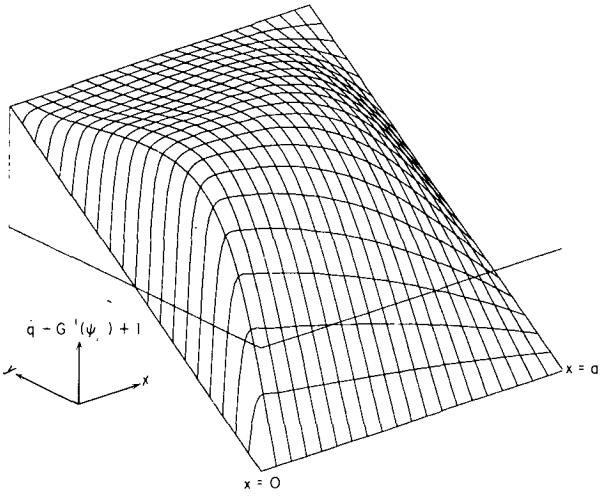

FIG. 6. $q - G^{-1}(\psi_2) + 1$ with G calculated using the boundary layer matching argument; see (3.21). The agreement between theory and numerical calculation is indicated by the plateau in the northwest corner of the basin which coincides with the closed q contours.

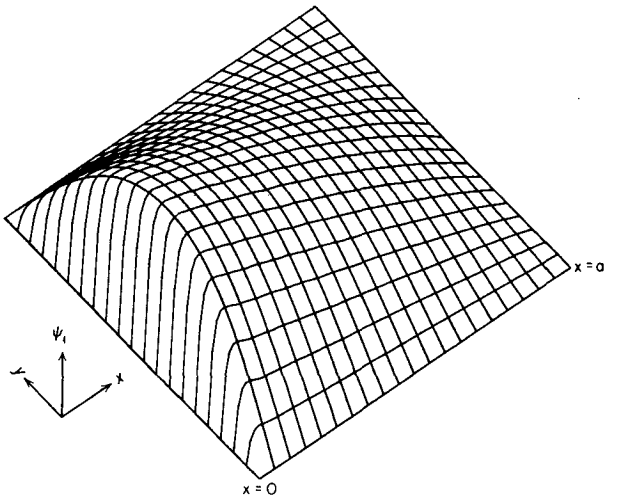

FIG. 7. The upper layer streamfunction ψ_1.

6. Conclusion

The simple model discussed is intended to emphasize a possibility which did not arise in the regime studied by YR and RY—the failure of the Prandtl–Batchelor theorem due to the passage of every streamline through a frictional boundary layer.

It is likely, however, that this theorem *does* apply to interesting and complicated systems. One of its clearest predictions is that the potential vorticity will be uniform in certain parts of a wind-driven gyre. This notion is supported by both ocean observations (McDowell *et al.*, 1982; Coats, 1981) and numerical experiments (Holland, 1983; McWilliams and Chow, 1981; Bleck and Boudra, 1981).

If the above results are accepted as successful ap-

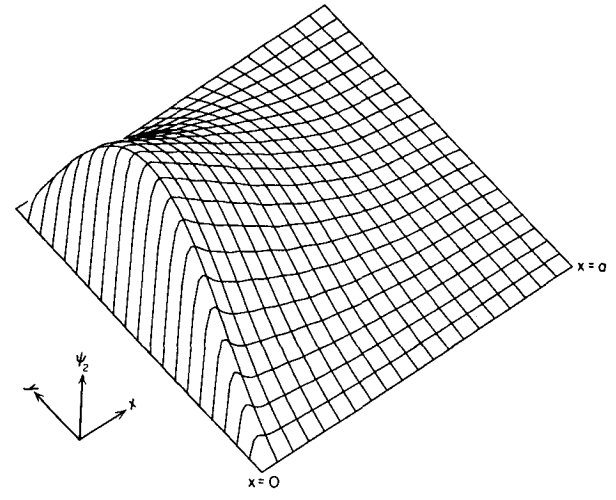

FIG. 8. The lower layer streamfunction ψ_2. Outside the region of closed q contours ψ_2 is small [$O(\nu, \delta)$].

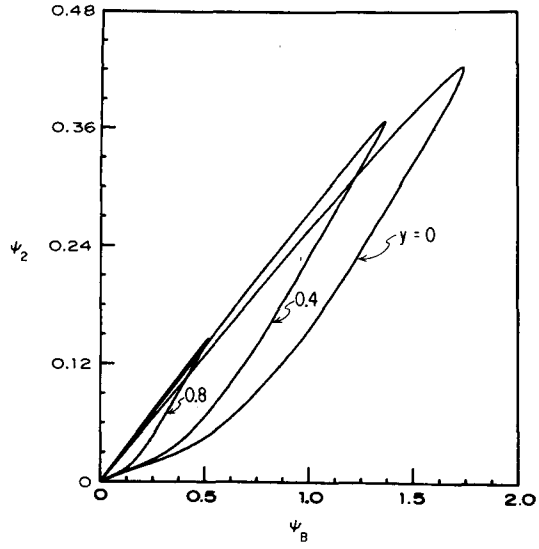

FIG. 9. Streamfunctions ψ_2 versus ψ_B on several east–west sections across the gyre. On each section the relationship encloses an approximately triangular region in the ψ_2–ψ_B plane. The three sides of the triangle correspond to passage through three different dynamical regimes: the western boundary layer, closed geostrophic contours and blocked geostrophic contours (see Fig. 11).

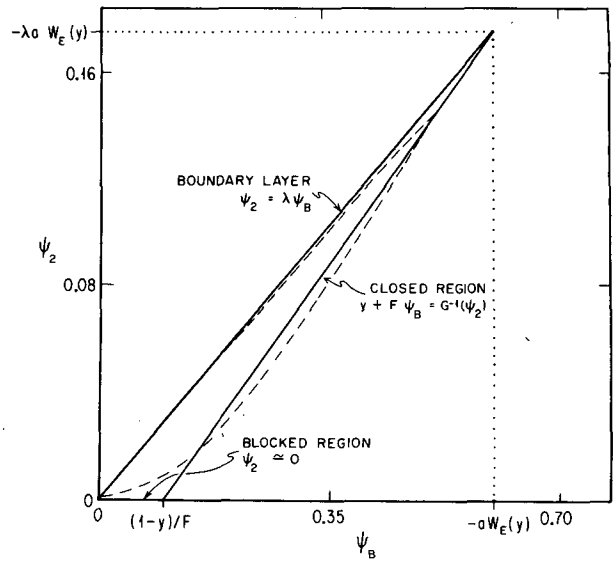

FIG. 11. The theoretically predicted relationship between ψ_2 and ψ_B (solid triangle) compared with the numerically calculated relation (dashed curve) at $y = 0.8$ and $\delta = 0.1$.

plications of the theorem then the present study raises several questions. Does the inclusion of relative vorticity (and the consequent development of inertial boundary layers where $q_y > 0$) alter the dynamics so that (1.1) is valid everywhere? This question can be answered by restoring the relative vorticity in (2.2) and solving the resulting system numerically. In numerical experiments, such as Holland (1982), how exactly does (1.1) hold in the western boundary layer?

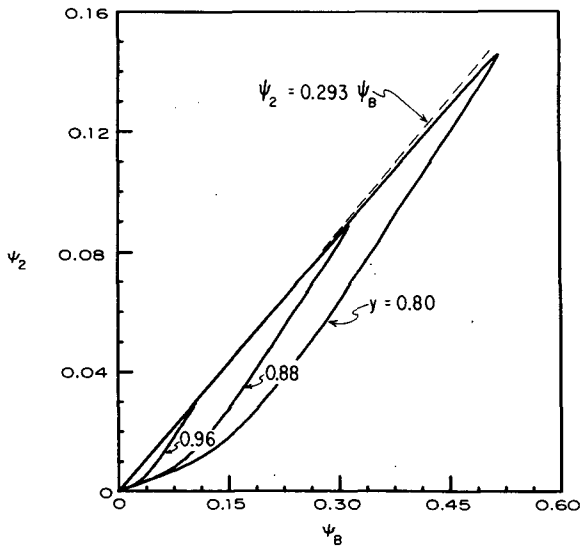

FIG. 10. Streamfunctions ψ_2 versus ψ_B on several northerly zonal sections. Note that the slope of the linear relation between ψ_2 and ψ_B in the boundary layer is independent of y and is very close to the theoretical value of 0.293. As one moves south the slope departs slightly from this value (see Fig. 9).

Acknowledgments. We thank Peter Rhines for much encouragement and discussion during the course of this work. Dr. Anthony Roberts made several constructive suggestions and forced W.R.Y. to abandon some rather wishful thinking.

W.R.Y. was supported by the National Science Foundation Grant OCE-80-23763, W.H.O.I. Summer Study Program in Geophysical Fluid Dynamics and ONR Grant N00014-79-C-0472. G.R.I. thanks the MIT Mathematics Department for the use of their computation facilities.

We thank Jo Griffith and the flat-bed plotter for their superb illustrations and Regina Hagen for her perserverance in typing this manuscript.

APPENDIX

An Erroneous Application of the Prandtl–Batchelor Theorem

We begin by integrating (3.4a) over the area enclosed by a closed q contour. The Jacobian term vanishes leaving

$$\nu \int \nabla\psi_B \cdot \hat{\mathbf{n}}\, dl = (2\nu + \delta) \int \nabla\psi_2 \cdot \hat{\mathbf{n}}\, dl \qquad \text{(A1)}$$

where $\hat{\mathbf{n}}$ is the unit normal to the contour. Now suppose (incorrectly) that (3.7) applies everywhere around the closed q contour. Substituting this into (A1) and using

$$\int \hat{\mathbf{y}} \cdot \hat{\mathbf{n}}\, dl = 0$$

gives the incorrect result (3.9). It is important to note that (A1) is correct and exact, and the error resides in the incorrect substitutions.

REFERENCES

Bleck, R., and D. B. Boudra, 1981: Initial testing of a numerical ocean circulation model using a hybrid (quasi-isopycnic) vertical coordinate. *J. Phys. Oceanogr.*, **11**, 755–779.

Coats, D. A., 1981: An estimate of absolute geostrophic velocity from the density field in the northeast Pacific Ocean. *J. Geophys. Res.*, **86**, 8031–8036.

Gadzag, J., 1976: Time-differencing schemes and transform methods. *J. Comput. Phys.*, **30**, 196–206.

Gottlieb, D., and S. A. Orszag, 1977: *Numerical Analysis of Spectral Methods.* SIAM, Philadelphia, 172 pp.

Haidvogel, D. B., and T. Zang, 1979: The accurate solution of Poisson's equation by expansion in Chebyshev polynomials. *J. Comput. Phys.*, **30**, 167–180.

Holland, W. R., 1983: Regions of uniform potential vorticity in an ocean circulation model with mesoscale resolution. (In preparation.)

McDowell, S., P. B. Rhines and T. Keffer, 1983: Maps of North Atlantic potential vorticity and its relation to the general circulation. (submitted to) *J. Phys. Oceanogr.*

McWilliams, J. C., and J. H. S. Chow, 1981: Equilibrium geostrophic turbulence I. A reference solution in a β-plane channel. *J. Phys. Oceanogr.*, **11**, 921–949.

Munk, W. H., 1950: On the wind-driven ocean circulation. *J. Meteor.*, **7**, 79–93.

Needler, G. T., 1967: A model for thermohaline circulation in an ocean of finite depth. *J. Mar. Res.*, **25**, 329–342.

Pedlosky, J., 1979: *Geophysics Fluid Dynamics,* Springer-Verlag, 624 pp.

Rhines, P. B., and W. R. Holland, 1979: A theoretical discussion of eddy driven mean flows. *Dyn. Atmos. Oceans,* **3**, 289–325.

——, and W. R. Young, 1982a: A theory of the wind-driven circulation I. Mid-ocean gyres. *J. Mar. Res.*, **40**(Suppl.), 559–596.

——, and ——, 1982b: Homogenization of potential vorticity in planetary gyres. *J. Fluid Mech.*, **122**, 347–367.

Stommel, H., 1948: The westward intensification of wind-driven ocean currents. *Trans. Amer. Geophys. Union.*, **29**, 202–206.

Welander, P., 1966: A two-layer frictional model of wind-driven motion in a rectangular oceanic basin. *Tellus,* **18**, 54–62.

——, 1968: Wind-driven circulation in one- and two-layer oceans of variable depth. *Tellus,* **20**, 1–15.

Young, W. R., 1980: What determines the vertical structure of the general circulation? 1980 Summer Study Program in Geophysical Fluid Dynamics. W.H.O.I. Tech. Rep.

——, and P. B. Rhines, 1982: A theory of the wind-driven circulation II. Circulation models and western boundary layers. *J. Mar. Res.*, **40**, 849–872.